Journal of Power Sources 195 (2010) 2592–2598

Contents lists available at ScienceDirect

Journal of Power Sources

journal homepage: www.elsevier.com/locate/jpowsour

Annealing induced interfacial layers in niobium-clad stainless steel developed as a bipolar plate material for polymer electrolyte membrane fuel cell stacks

Sung-Tae Hong[a,*], K. Scott Weil[b,**], In-Tae Bae[c], Jung Pyung Choi[b], Jwo Pan[d]

[a] School of Mechanical and Automotive Engineering, University of Ulsan, 29 Mugeo 2 Dong, Nam Gu, 680-749 Ulsan, South Korea
[b] Pacific Northwest National Laboratory, Richland, WA 99352, USA
[c] Small Scale Systems Integration and Packaging Center, Binghamton University, Binghamton, NY 13902, USA
[d] Mechanical Engineering, University of Michigan, Ann Arbor, MI 48109, USA

ARTICLE INFO

Article history:
Received 13 August 2009
Received in revised form 8 September 2009
Accepted 9 October 2009
Available online 23 October 2009

Keywords:
Cladding
Bipolar plate
Proton exchange membrane fuel cell
Annealing

ABSTRACT

Roll-bonded niobium (Nb)-clad 304 L stainless steel (SS) is currently being developed as a metallic bipolar plate material for polymer electrolyte membrane fuel cell stacks. Prior work has shown that post-roll annealing significantly softens the constituent core and cladding materials, enhancing the ductility and formability of each. However under the vacuum annealing condition employed in the previous study (900 s, 982 °C (1800 F)), an interfacial layer was observed to form between the two bonded materials. Subsequent bending and flattening tests indicated brittle failure of this interfacial region under high strain conditions. The present study employs transmission electron microscopy to examine the composition, structure, and thickness of phases generated at the Nb/SS interface as functions of annealing temperature and time. Corresponding selected electron diffraction patterns indicate that above a threshold annealing temperature of ~950 °C, the formation of $(Fe_{1-x}Cr_x)_2Nb$ appears to control the failure behavior of the Nb/304 L SS material. Annealing treatments conducted below this temperature generally avoid the formation of this intermetallic layer.

1. Introduction

In spite of the significant technical progress made in recent years toward developing a commercially viable polymer electrolyte membrane fuel cell (PEMFC) system, the use of PEMFCs in automotive applications is still limited to prototypes [1]. The reasons for their limited use in automobiles include the high cost of PEMFC stack manufacture and the steady loss in power output typically observed during long-term continuous operation. Fuel cells are currently five times more expensive than internal combustion engines (ICEs) and do not maintain performance over the full useful life of the vehicle. In addition, the current size and weight of PEMFC stacks limit the specific power that can be generated [2], which is one of the key parameters for transportation application. It is clear that a reduction in cost and improvements in performance must come from all aspects of PEMFC system design and manufacture for this technology to be competitive with current ICEs and future alternative power sources in the automotive market sector.

One of the most bulky components in a PEMFC stack with respect to both weight and volume is the bipolar plate [3]. This component serves not only as the electrical junction between the serially connected cells within the stack, but also performs several other key functions in the overall system [4], including:

- Distributing fuel and oxidant uniformly over the active areas of the cells;
- Facilitating water management within the stack to maintain proper membrane humidification, yet avoid flooding;
- Serving as an impermeable barrier between the fuel and oxidant streams to maintain the hydrogen gradient across the membrane necessary for high power output;
- Providing structural support for the stack;
- Removing heat from the active areas of the cells.

In the early days of PEMFC development, graphite was the material of choice for use in the bipolar plate because of its excellent corrosion resistance and surface conductivity in the low pH/hot aqueous environment (60–80 °C) of the stack. However, the high cost and brittle nature of high purity graphite and the expense associated with machining individual plates necessitated the development of lower cost bipolar plate materials for commercial applications. Among these, the leading candidates have been

* Corresponding author. Tel.: +82 52 259 2129.
** Corresponding author. Tel.: +1 509 376 6796.
E-mail addresses: sthong@ulsan.ac.kr (S.-T. Hong), scott.weil@pnl.gov (K.S. Weil).

0378-7753/$ – see front matter © 2009 Elsevier B.V. All rights reserved.
doi:10.1016/j.jpowsour.2009.10.034

graphite- or carbon-based composites and metal alloys in both uncoated and coated forms.

However, to date, the use of polymer impregnated graphite- and carbon-composite bipolar plates has been beset by several problems of particular concern in an automotive application: (1) the resulting bipolar plates are bulky because they need to be several millimeters thick to ensure gas impermeability and acceptable strength; (2) due to low material toughness, the plates require careful handling to avoid damage prior to assembly; (3) injection molded composite plates have a design-restrictive trade-off associated with particulate loading, i.e., electrical conductivity versus proper polymeric flow during molding; and (4) alternatively compression molded plates, while offering greater bulk conductivity due to higher particulate loadings, are far more difficult and expensive to manufacture [5].

By comparison, metal alloys offer a number of attractive advantages for automotive PEMFC systems including:

- Low-cost, mass-production via stamping or embossing of sheet product;
- Fabrication in very thin form (<150 μm) to reduce the weight and volume in the overall PEMFC stack;
- Impermeability to fuel, oxidant, and water vapor;
- Excellent thermal conduction properties;
- Good mechanical robustness.

However, a potential show-stopper with any metal-based stack component is surface corrosion, and the current drive to increase the operating temperature of the stack will only exacerbate this problem. Corrosion of the bipolar plate leads to a release of metal ions that can contaminate the electrolyte membrane and poison the electrode catalysts, thereby exaggerating the long-term degradation issues with PEMFC stacks [6,7]. In addition, the formation of a passivating oxide or oxyhydroxide layer on the surface of the metal tends to increase the contact resistance between the bipolar plate and the adjacent carbon-based gas diffusion layer (GDL), often by many orders of magnitude, which both limits the amount of power that can be generated by the stack and serves as an additional source of heat that must be removed during operation.

A clad metal material was recently developed, which appears to overcome these deficiencies and is sufficiently robust for use in automobiles [8]. In its current form, the material is comprised of a thin 12.5 μm layer of commercially pure niobium (cp-Nb) roll bonded to a thicker (125 μm) 304 L stainless steel (SS) sheet, although recent processing results suggest that the thickness of the Nb sheet can be further reduced by roll bonding to 4–5 μm. Results from linear voltammetry and potentiostatic testing conducted under aggressive conditions (80 °C in 1 M H_2SO_4 + 2 ppm HF) demonstrated that the material is electrochemically viable, exhibiting passivating behaviors with current densities that are comparable (at typical anode and cathode potentials) to those of non-corrosive noble metals such as Pt [9]. Measurements of the contact resistance between a representative Toray™ GDL paper and the Nb side of the clad sheet in the as-received or passivated conditions were comparable to previously reported values for graphite [9]. Preliminary mechanical property characterization of the clad material in the as-rolled and post-roll annealed conditions indicated that annealing may be required to restore sufficient ductility for the subsequent blanking, stamping, and bending operations needed to form the final bipolar plate configuration [10]. However the annealing step employed in that study (a high vacuum annealing at 982 °C for 900 s) led to the formation of an interfacial layer between the Nb cladding and the SS substrate.

It was found that the interfacial layer played a key role in the failure of the annealed Nb-clad 304 L SS [10]. Failure in the annealed Nb-clad 304 L SS under bending/tension initiated via brittle fracture of the interfacial layer, forming a series of periodically spaced internal cracks. These internal cracks eventually formed internal pores that initiated necking and through-thickness failure in the Nb cladding layer at larger material strains. For this material to be considered viable for commercial application, particularly when the thickness of the niobium cladding is reduced to <5 μm, it must be formable via low-cost (often moderate-to-high strain) processes such as stamping and bending. Thus the objectives of this follow-up study were to: (1) identify the nature of the interfacial layer and determine the heat treatment conditions under which it forms and thickens and (2) define conditions under which annealing can be conducted without the formation of this deleterious layer.

2. Experimental set-up

The experiments were conducted on Nb-clad 304 L SS sheets fabricated via roll bonding by Engineered Materials Solutions Inc. (EMS; Waltham, MA). The roll bonding conditions were chosen with the intent of preparing an as-rolled baseline material that does not exhibit formation of an interfacial layer. Thus, the roll pressure, roll speed, and backward and forward tensions on the incoming and outgoing sheet were adjusted to levels deemed just high enough to avoid delamination of the niobium layer from the stainless steel substrate without inducing substantial internal heating and subsequent spontaneous generation of an interfacial reaction layer. Multiple passes were employed to achieve a thickness reduction of 95.6%. As a result, the materials investigated in the present study were approximately four times thicker (1.12 mm) than those examined in Hong and Weil [10] (0.254 mm). Table 1 lists the cold rolling parameters of the Nb-clad 304 L SS used in this investigation. As will be discussed later, no reaction product layers or precipitates were observed along the Nb/SS interface of the baseline as-rolled material. Since the baseline as-rolled material used in this research was too thick to be used in the manufacture of commercial PEMFC bipolar plates, the evaluation of the effect of annealing on the mechanical properties was not considered here. The relationship between the two will be examined in a subsequent process optimization study using material with a prototype thickness.

Annealing was conducted under a range of conditions considered to be appropriate for cp-Nb and/or 304 L SS. In the case of cp-Nb, the annealing atmosphere must be free of hydrogen to avoid embrittlement, particularly during the cooling portion of the heat treatment cycle [11]. As a rule, austenitic stainless steels generally must be rapidly cooled from the annealing temperature (often by water quenching) to prevent sensitization, or the loss of chromium in the alloy through the formation of chromium carbides [11]. However, since 304 L SS is a low carbon alloy, it can be cooled slowly without concern of carbide precipitation [12]. Thus the Nb-clad 304 L sheets were annealed in a hydrogen-free, high vacuum environment and allowed to furnace cool from the annealing soak temperature to room temperature.

The typical temperature ranges used for annealing cp-Nb and 304 L SS are shown in Fig. 1. As seen in Fig. 1, the minimum temperature required for stress-relieving cp-Nb is approximately 800 °C and the temperature range for recrystallization annealing of cp-Nb is 900–1200 °C [11]. The recommended temperature range for annealing 304 L SS is 1010–1120 °C [12]. Three different annealing temperatures, 850, 950, and 1050 °C, were chosen to represent each of these heat treatment ranges. The annealing temperatures of 850 and 950 °C were selected even though they are lower than the minimum annealing temperature recommended for 304 L SS, since the primary objective in annealing the Nb-clad SS is to regain the ductility of the Nb cladding layer to manufacture bipolar plates without defects in the protective Nb cladding layer. Annealing times of 15 and 60 min were chosen as representative short and long period

Table 1
The cold rolling parameters of the Nb-clad 304 L SS.

Materials	Thickness prior to rolling (mm)		Total thickness after final rolling (mm)	Total thickness reduction (%)
	SS	Nb		
5%Nb-clad 304 L SS	1.27	24.13	1.12	−95.6

Table 2
The annealing conditions for the Nb-clad 304 L SS.

Test number	Temperature (°C)	Time (min)
1	850	15
2	950	15
3	1050	15
4	850	60
5	950	60
6	1050	60

annealing runs, respectively. The six different annealing conditions employed in the present study are listed in Table 2. In each run, samples were heated from room temperature to the target soak temperature over a 1-h period.

Microstructural analyses of the materials before and after annealing were conducted on polished cross-sectioned samples using a JEOL JSM-5900LV scanning electron microscope (SEM) equipped with an Oxford energy dispersive X-ray analysis (EDX) system. Elemental profiles were also recorded across each clad/core interface in the line-scan mode. In addition, a focused ion beam (FIB) *in situ* lift-out technique was employed to extract electron transparent samples from select heat treatment specimens using a FEI Helios Nanolab dual-beam FIB/SEM. Compositional and structural details on these samples were investigated using a JEOL JEM-2010 transmission electron microscope (TEM) operated at 200 kV and equipped with an Oxford EDX system.

3. Results

A cross-sectional back-scattered electron image of the baseline as-rolled Nb-clad 304 L SS material is shown in Fig. 2. Results from elemental line scans of niobium, nickel, iron, and chromium across the clad/core interface are superimposed on the micrograph. It is apparent that roll bonding yielded a metallurgical bond between the niobium-clad and underlying stainless steel core, as evidenced by the lack of interfacial porosity. No reaction layer or inclusions were observed in this specimen. Diffusion between the clad and core layers appeared to be limited to a narrow ~1.5 μm thick region across the bondline, as estimated from the dimension over which each elemental profile changed from its maximum to minimum value.

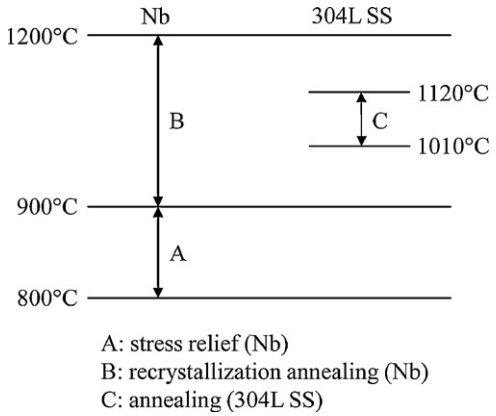

Fig. 1. The temperature ranges for annealing of pure Nb and 304 L SS.

Shown respectively in Fig. 3(a)–(f) are cross-sectional back-scattered electron images of the Nb-clad 304 L SS specimens annealed at 850 °C/15 min, 850 °C/60 min, 950 °C/15 min, 950 °C/60 min, 1050 °C/15 min, and 1050 °C/60 min. Again, results from elemental line scans across the clad/core interface are superimposed on each respective image. As seen in Fig. 3(a) and (b), the Nb/SS interface remained relatively sharp after vacuum annealing at 850 °C, even for a period as long as 60 min. The width of the intermediary diffusion zone increased by only 10–15% from that of the original as-rolled condition. A similar phenomenon was observed in the specimen annealed at 950 °C for 15 min as seen in Fig. 3(c). In all four cases (including the as-rolled specimen in Fig. 2), the elemental gradients were smooth and continuous. However for the last three heat treatments, 950 °C/60 min, 1050 °C/15 min, and 1050 °C/60 min, shown in Fig. 3(d)–(f), respectively, there are obvious differences in the image contrasts and corresponding discontinuities in the compositional gradients, which suggest new phase formation.

In particular for the specimens annealed at 1050 °C, there appear to be two new interfacial regions distinguishable by a difference in back-scattered electron contrast. In the elemental line scans for both of these specimens, there is a region of zero slope (i.e. a concentration isopleth) which suggests the formation of an intermetallic compound of invariant composition. In comparison, no such zero slope region is observed in the elemental line scans for the 950 °C/60 min specimen in Fig. 3(d), although there are apparent breaks in slope. Also noted is an increase in the thickness of the interfacial diffusion and/or reaction zones with increased temperature and time at temperature. This is shown more directly by the plot in Fig. 4, which is based on estimates from the EDX data.

Re-drawn as a process map in Fig. 5, this information suggests conditions under which the roll-bonded Nb-clad 304 L SS can be vacuum annealed without forming a potentially brittle intermetallic reaction layer. Results from EDX analyses conducted at points within the apparent intermetallic regions of the 1050 °C/15 min and 1050 °C/60 min specimens are listed in Table 3 and correspond respectively to Points 1 and 2 in Fig. 3(e) and (f). Also, the EDX

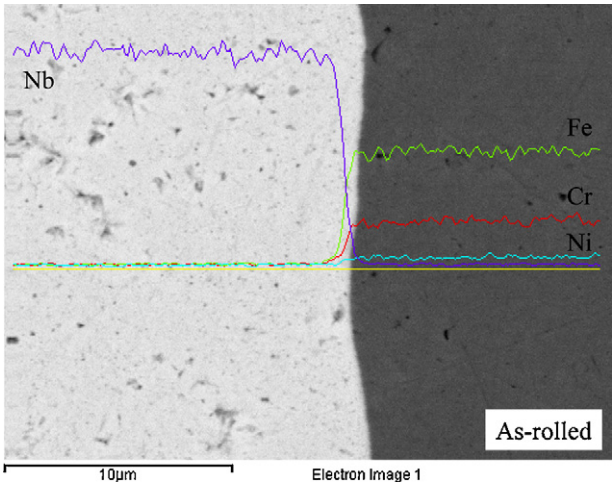

Fig. 2. A cross-sectional back-scattered electron image of the baseline as-rolled Nb-clad SS specimen with the results of elemental line scans across the clad/core interface.

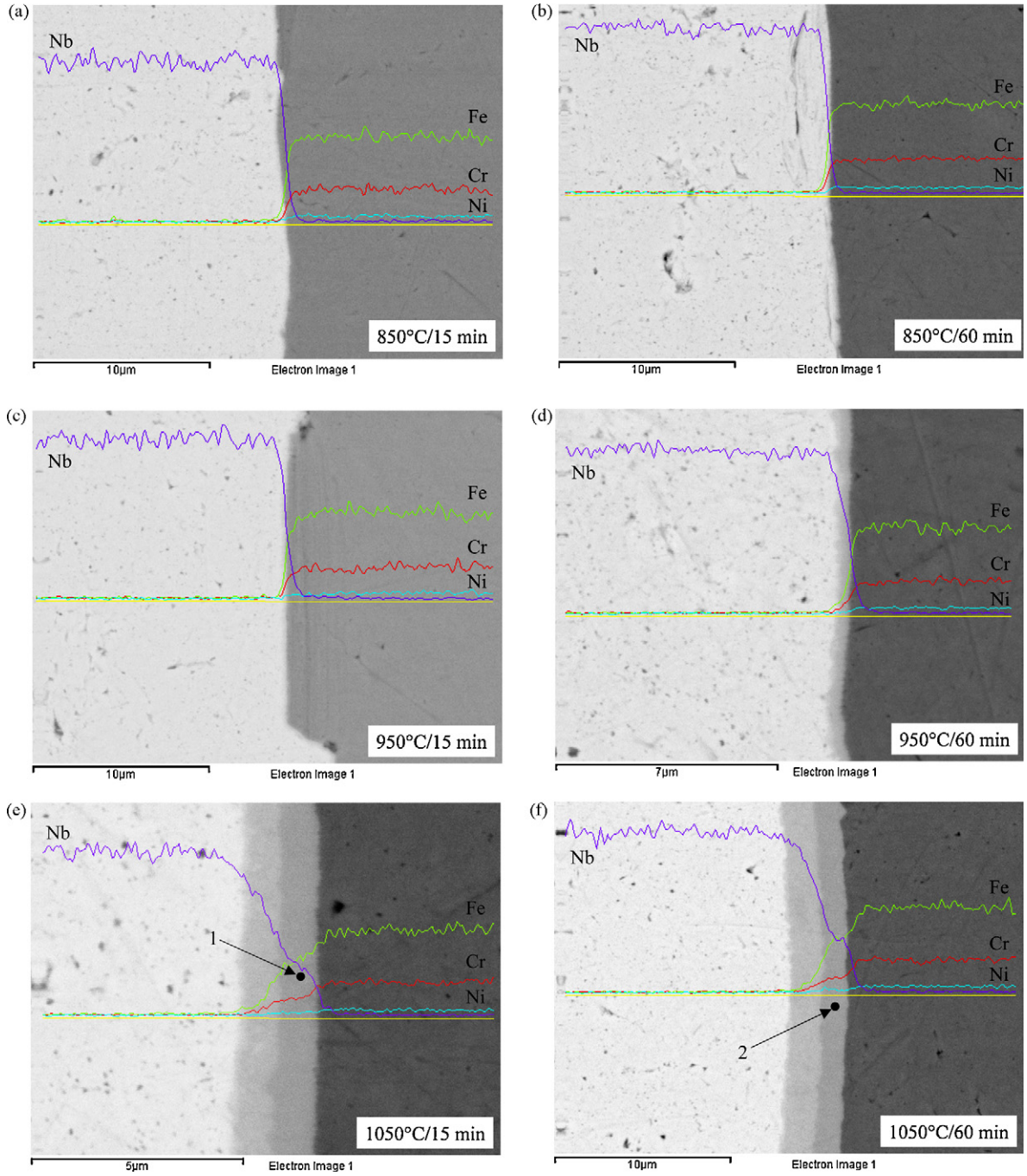

Fig. 3. Cross-sectional back-scattered electron images of the Nb-clad SS specimens annealed at (a) 850 °C/15 min, (b) 850 °C/60 min, (c) 950 °C/15 min, (d) 950 °C/60 min, (e) 1050 °C/15 min, and (f) 1050 °C/60 min with the results of elemental line scans across the clad/core interface.

results reported in Hong and Weil [10] for the Nb-clad 304 L SS specimen annealed at 982 °C for 15 min are listed in Table 3 for comparison. Again, this information was recorded for a region of invariant composition associated with an obvious interfacial band within the specimen. Based on the limited chemical data taken in that study [10], the reaction layer was speculated to be composed of the intermetallic η-phase Fe_2Nb_3. However, the layers of interest in the present study display a significantly higher iron-to-niobium ratio.

To understand the nature of this interface more clearly, detailed structural analysis was conducted by TEM on a piece of the multi-layered region cut by FIB from the specimen annealed at 1050 °C for 60 min. Shown in Fig. 6(a) is a scanning TEM bright-field image of the multi-layered region overlaid with results from EDX elemental line-scan analysis. Interestingly, the interface consists of not two but three distinct zones, denoted as I, II, and III. Zones I and II correspond to the distinct layer adjacent to the Nb side of the specimen

Table 3
The chemical compositions of the intermetallic layers.

Materials	Composition (at.%)			
	Fe	Cr	Ni	Nb
1050 °C/15 min	52.16	13.47	4.80	29.58
1050 °C/60 min	52.37	12.34	5.56	27.52
982 °C/15 min [10]	37.85	8.82	4.07	48.74

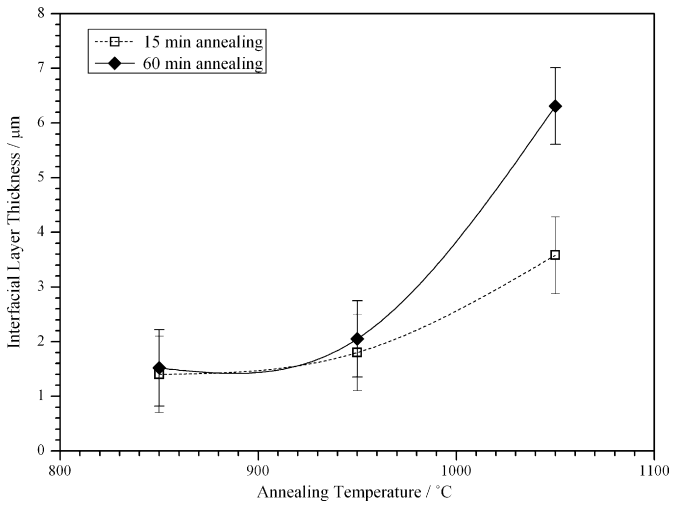

Fig. 4. The interfacial layer thickness (i.e. diffusion zone width + reaction layer width) as a function of annealing temperature.

in Fig. 3(f), while Zone III is the layer adjacent to the SS side in the same micrograph. As seen in Fig. 6(a), Zone I is composed of columnar niobium grains 1–1.5 μm long oriented perpendicular to the cp-Nb/Zone I interface. While the EDX data indicate little diffusion of iron, chromium, or nickel into this region, it should be noted that very small concentrations (<0.5 at.%) of these first row transition metals can significantly affect the grain size and grain morphology in unalloyed versions of early transition metals [13]. It is suspected that a small amount of iron, chromium, or nickel diffusion not measurable by the EDX technique used in the present study altered recrystallization of the abutting niobium and caused columnar grain growth during annealing. Approximately linear concentration gradients are observed in Zone II for all of the elements measured, indicating alloying but no reaction occurring in this region of the specimen. The concentration of each element reaches a constant value in Zone III, which signals the formation of an intermetallic compound in this layer and is consistent with the results in Fig. 3(f).

Shown in Fig. 6(b) is a bright-field TEM image of Zone III. The material in this region exhibits equiaxed grains that are sub-micron in size. As denoted by the arrows in the micrograph, numerous

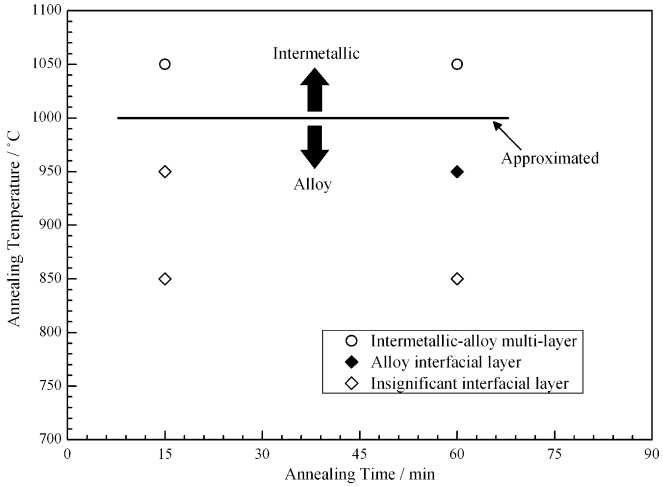

Fig. 5. A process map for the interfacial layer development as functions of the annealing temperature and time. The approximate border line for the development of multiple-layered interfacial layers in which the layer with a nearly constant chemical composition exists is also shown.

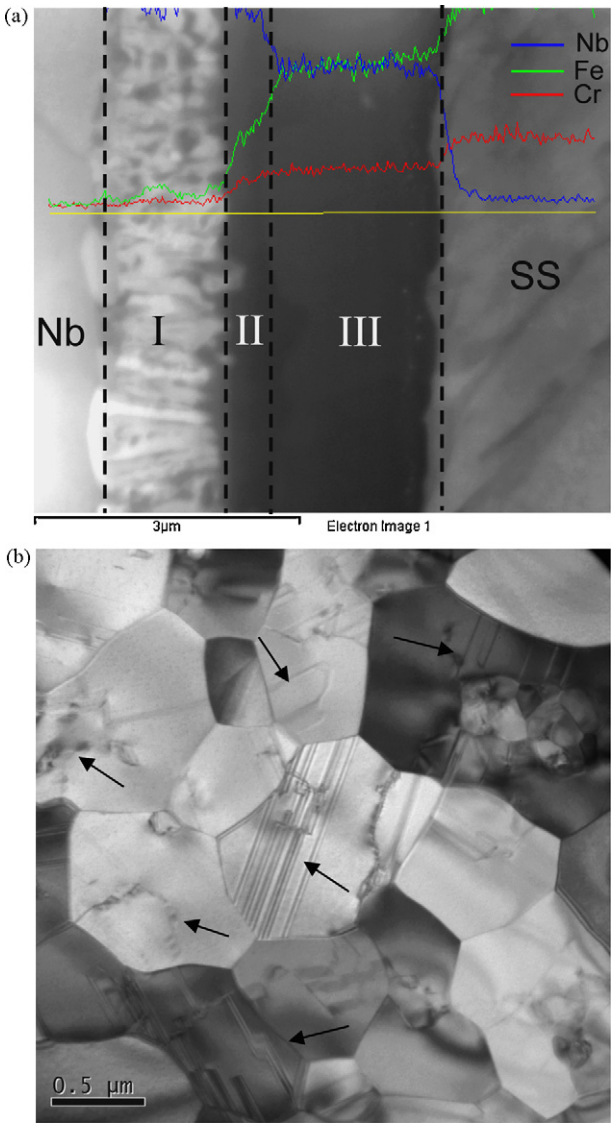

Fig. 6. TEM bright-field images of the specimen annealed at 1050 °C/60 min: (a) a cross-sectional view across the entire interfacial layer with the results from elemental line scans superimposed and (b) a cross-sectional view of Zone III.

defects such as stacking fault defects and dislocation structures can be seen. Selected area electron diffraction (SAED) was conducted to determine the crystal structure of the material in this zone and typical patterns are shown in Fig. 7. The structure factor, F_{hkl} (where hkl represents a specific Bragg reflection), was calculated for all known intermetallic phases consisting of iron, nickel, chromium, and niobium. Calculations of the electron diffraction patterns were based on the following kinematical approximation [14]:

$$F_{hkl} = \sum_n f_n \exp[2\pi i(hx_n + ky_n + lz_n)] \quad (1)$$

where f_n is the atomic scattering factor for atom n at fractional coordinates (x_n, y_n, z_n).

A comparison of the recorded diffraction patterns shown in Fig. 7(a)–(c) with the corresponding simulations calculated from Eq. (1) in Fig. 7(a′)–(c′) indicates that the dominant phase in Zone III exhibits the crystal structure of Fe_2Nb and Cr_2Nb (space group of $P6_3/mmc$, prototype structure of Zn_2Mg, C14 Strukturbericht designation). The simulations shown are for pure Cr_2Nb. However the same patterns were found for Fe_2Nb with minor changes in the spot intensity. Note that the extra intensity maxima observed in

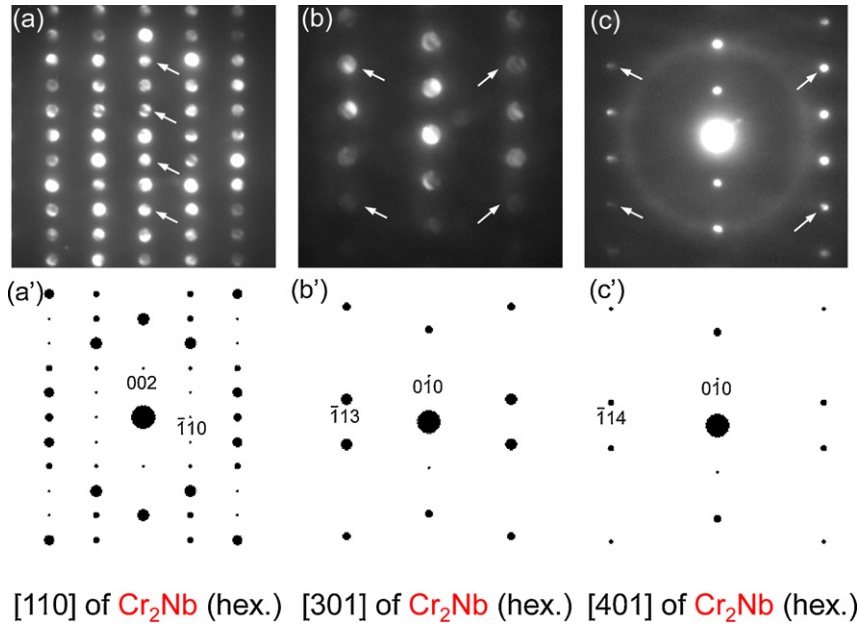

Fig. 7. SAED patterns obtained from individual grains in Zone III (a)–(c). Simulation results for electron diffraction patterns along the following axes for a hexagonal C14 Laves phase (AB_2) with Cr in the B-site and Nb in the A-site Wyckoff positions: (a′) [1 1 0], (b′) [3 0 1], and (c′) [4 0 1].

Fig. 7(a)–(c) (indicated by arrows) are attributed to multiple electron scatterings.

Fe_2Nb is thermodynamic stable at 1050 °C, but is not a line compound and can exhibit a significant degree of non-stoichiometry, from 27 to 38 at.% Nb with Nb substitution occurring on the Fe Wyckoff positions for Nb-rich forms of the compound and vice versa [14]. Similarly Cr_2Nb exhibits a wide compositional range. However the hexagonal C14 phase of Cr_2Nb is not stable below ~1585 °C [15]. Instead the cubic C15 Laves structure is the stable form at 1050 °C. This information and the corresponding EDX data in Fig. 6(a) suggest that the intermetallic phase that formed in the 1050 °C annealed specimen is iron-based, likely with a significant amount of random chromium substitution, i.e. $(Fe_{1-x}Cr_x)_2Nb$. Transition metal substitutions of this type are not uncommon in cubic and hexagonal Laves phase compounds and have been reported for the intermetallic precipitates of various alloy systems [16,17], as well as single phase compounds [18]. Recently Zhu et al. [19] reported that the substitution of Fe for Cr stabilizes the hexagonal C14 structure in the $Nb(Cr,Fe)_2$ system. This is due to increased electron concentration in the intermetallic compound, which agrees with the combined TEM/EDX/SAED results in the present study. As a final comment, the bulk resistance of the Nb-clad material was measured in the as-rolled and annealed conditions via a four-point technique using an Agilent 34410A Multimeter. No significant change in bulk resistance was observed upon annealing, regardless of the annealing conditions.

4. Conclusion

Roll-bonded Nb-clad 304 L SS has showed stable electrochemical properties for PEMFC bipolar plate application [9]. However, prior work [10] indicated that under certain annealing conditions a brittle reaction layer will form along the Nb/SS interface, which can have a deleterious effect on material formability. The present study examined in greater detail the conditions under which this reaction layer formed, identified the nature of this layer, and defined conditions under which the clad material could be annealed while avoiding reaction layer formation. Results from SEM and EDX analyses indicated that an annealing temperature of 850 °C safely avoids generating an interfacial layer at annealing times as long as 60 min. An annealing condition of 10 min at 950 °C could also be prescribed without interlayer formation. However longer annealing times at this temperature or alternatively carrying out annealing at higher temperatures tended to produce a thin interfacial reaction layer. Combined TEM/EDX/SAED analyses demonstrated that this layer is actually composed of three distinct zones: (I) 1–1.5 μm long columnar niobium grains oriented perpendicular to the Nb/SS interface, (II) a 0.5-μm wide alloy region that contains Nb, Fe, Cr, and Ni, and (III) an iron–chromium–niobium intermetallic compound, $(Fe_{1-x}Cr_x)_2Nb$, crystallizing in the hexagonal C14 structure. It is the latter phase that causes failure of improperly annealed Nb/304 L SS under high strain conditions.

Acknowledgements

The authors thank Steve Chang at Engineered Materials Solutions, Inc. for providing the clad materials and for his technical assistance in the study. This work was supported by the research fund of the University of Ulsan. This work was also supported by the U.S. Department of Energy, Office of Energy Efficiency, and Renewable Energy. The Pacific Northwest National Laboratory is operated by the Battelle Memorial Institute for the United States Department of Energy (U.S. DOE) under Contract DE-AC06-76RLO 1830.

References

[1] M. Lin, Y. Cheng, M. Lin, S. Yen, Evaluation of PEMFC power systems for UPS base station applications, J. Power Sources 140 (2005) 346–349.
[2] X. Li, I. Sabir, Review of bipolar plates in PEM fuel cells: flow-field designs, Int. J. Hydrogen Energy 30 (2005) 359–371.
[3] U.S. Department of Energy, Hydrogen, Fuel Cells & Infrastructure Technologies Program Multi-Year Research, Development and Demonstration Plan (2003–2010), Available from: http://www.eere.energy.gov/hydrogenandfuelcells/mypp.
[4] A. Hermann, T. Chaudhuri, P. Spagnol, Bipolar plates for PEM fuel cells: a review, Int. J. Hydrogen Energy 30 (2005) 1297–1302.
[5] G. Rinn, S. Bornbaum, Graphite bipolar plates for PEM fuel cells, Ceram. Forum Int. 82 (2005) E33–E36.
[6] R. Hornung, G. Kappelt, Bipolar plate materials development using Fe-based alloys for solid polymer fuel cells, J. Power Sources 72 (1998) 20–21.
[7] J.A. Sawicki, T. Tyliszczak, F.E. Wagner, J.H. Rolston, A.P. Hitchcock, D.E. Clegg, EXAFS and Mössbauer analysis of Pt–Ir catalysts, Physica B 158 (1989) 203–205.
[8] K.S. Weil, J.Y. Kim, G.G. Xia, Z.G. Yang, Clad metal material for PEMFC bipolar plates, U.S. Patent Office, in review.

[9] K.S. Weil, G. Xia, Z.G. Yang, J.Y. Kim, Development of a niobium clad PEM fuel cell bipolar plate material, Int. J. Hydrogen Energy 32 (2007) 3724–3733.
[10] S.-T. Hong, K.S. Weil, Niobium-clad 304L stainless steel PEMFC bipolar plate material: tensile and bend properties, J. Power Sources 168 (2007) 408–417.
[11] ASM Handbook, vol. 4, Heat Treating, ASM International Metals Park, Ohio, 2004.
[12] ASM Handbook, vol. 13, Corrosion, ASM International Metals Park, Ohio, 2004.
[13] V.K. Gupta, D.-H. Yoon, H.M. Meyer III, J. Luo, Thin intergranular films and solid-state activated sintering in nickel-doped tungsten, Acta Mater. 55 (2007) 3131–3142.
[14] B.D. Cullity, Elements of X-ray Diffraction, second ed., Prentice-Hall, 2001.
[15] H.J. Goldschmidt, J.A. Brand, The constitution of the chromium–niobium–molybdenum system, J. Less-Common Met. 3 (1961) 44–61.
[16] M. Grujicic, S. Tangrila, O.B. Cavin, W.D. Porter, C.R. Hubbard, Effect of iron additions on structure of Laves phases in Nb–Cr–Fe alloys, Mater. Sci. Eng. A 160 (1993) 37–48.
[17] G.R. Speich, Precipitation of Laves phases from iron–niobium and iron–titanium solid solutions, Trans. Am. Inst. Mining Metal. Petr. Eng. 224 (1962) 850–858.
[18] J. Huot, E. Akiba, T. Ogura, Y. Ishido, Crystal structure, phase abundance and electrode performance of Laves phase compounds (Zr, A)$V_{0.5}Ni_{1.1}Mn_{0.2}Fe_{0.2}$ (A≡Ti, Nb or Hf), J. Alloys Compd. 218 (1995) 101–116.
[19] J.H. Zhu, C.T. Liu, P.K. Liaw, Phase stability and mechanical behavior of $NbCr_2$-based Laves phases, Intermetallics 7 (1999) 1011–1016.